Integrated Flexible Hybrid Silicone-Textile Dual-Resonant Sensors and Switching Circuit for Wearable Neurodegeneration Monitoring Systems

Integrated Flexible Hybrid Silicone-Textile Dual-Resonant Sensors and Switching Circuit for Wearable Neurodegeneration Monitoring Systems

Imran M. Saied, Siddharthan Chandran, and Tughrul Arslan, *Senior Member, IEEE*

***Abstract*— This paper describes the design, development, and testing of flexible hybrid silicone-textile sensors and a flexible switching circuit that were integrated into a wearable system for monitoring neurodegenerative diseases. A total of 6 planar monopole antenna sensors were fabricated that propagates at two separate resonant frequencies: 800 MHz and 2.1 GHz respectively. In addition, 2 switching circuits, each having 3 switches and 4 SMA breakout boards, were assembled and placed on the wearable neurodegeneration monitoring system. Each switching circuit connects 3 sensors to a single port on a vector network analyser (VNA) that is used to generate and receive microwave signals. Experiments were performed using the wearable device with the developed sensors and switching circuit on phantoms mimicking two common physiological changes in the brain caused by neurodegenerative diseases: 1) brain atrophy and 2) lateral ventricle enlargement. The dual nature of the sensors' resonance allows it to detect both brain atrophy and lateral ventricle enlargement separately at different operating frequency. This provides the advantage of minimising the number of sensor elements needed to monitor neurodegenerative disease. The use of a switching circuit also allows for quick and convenient measurements by choosing which sensors are active for ports 1 and 2 on the VNA respectively. In addition to being low-cost, the flexibility of the materials used in fabrication allows the sensors and switching circuit to be conformal to the patient's head. Results from the experiments indicates that the sensors and switching circuit were working successfully when integrated into the wearable device.**

***Index Terms*—Wearable electronics, wearable sensors, flexible circuits, microwave imaging, head diagnostic systems**

I. Introduction

NUERODEGENERATIVE diseases, such as Alzheimer's disease, is the progressive loss of neurons in the brain which results in the gradual loss of cognitive functions and eventually leads to death. Some of the key physiological symptoms that occur during neurodegeneration are faster rates of brain atrophy and lateral ventricle enlargement. One study shows that the mean whole-brain atrophy rate was -1.9 +/- 0.9% per year for patients with Alzheimer's disease as compared to healthy elderly people who have an average whole-brain atrophy rate of 0.44% per year [1],[2]. Several studies have also shown evidence of faster rates of lateral ventricle enlargement for patients with Alzheimer's disease, where the percentage increase could be anywhere between 3 to 5.5% per year [3], [4]. Current diagnostic tools such as MRI and CT scans are bulky, expensive, and can be difficult for patients to use. As a result, there is a need for more portable and wearable devices that will allow patients to comfortably wear and monitor the progression of neurodegeneration in their brain. In addition, having a portable and wearable technology for neurodegeneration monitoring can be efficient in obtaining measurements at the convenience of the patient while they are at home or in a clinic.

Microwave radar-based technology has been at the forefront of recent research techniques being investigated for head imaging systems. Compared to conventional diagnostic methods, microwave radar-based technology has the advantage of being inexpensive, lightweight, and non-ionising. Microwave imaging works by detecting differences in electrical properties between healthy and unhealthy human tissues. By measuring and collecting backward scatters from the head one can know the presence and location of unhealthy tissues in the brain. Microwave medical imaging has been used for stroke and cancer detection successfully [5],[6]. The authors have also developed and tested an initial wearable device, consisting of inkjet-printed antennas for detecting and monitoring brain atrophy and lateral ventricle enlargement, which is discussed in [7]. In that work, the minimum brain atrophy that could be detected by the antennas was 5%. In addition, the smallest

This paper was submitted on July 15, 2019, revised on September 21, 2019.
I. M. Saied and T. Arslan are with the School of Engineering, University of Edinburgh, Edinburgh, UK EH9 3JW (Email: Imran.Saied@ed.ac.uk, Tughrul.Arslan@ed.ac.uk)

S. Chandran is with the School of Medicine, University of Edinburgh, Edinburgh, UK EH9 3JW (Email: Siddharthan.Chandran@ed.ac.uk)

increase in lateral ventricle enlargement that could be detected was a volume increase of 22.6 mm^3. The work described in [7] was, to the authors' knowledge, the first study conducted for monitoring neurodegenerative disease using microwave sensing techniques. A microwave head imaging system typically consists of a device containing antenna sensors that are placed on the body under test, and a vector network analyser (VNA) that is used to generate and receive microwave signals from each of the antenna elements.

A key component of microwave head imaging systems are antennas that emit radiofrequency waves. Current research has focused on the development of wearable antennas for microwave head diagnostics systems. These antennas provide the benefits of being flexible, conformal and comfortable as compared to more rigid antennas. In [6] and [8], a Vivaldi antenna was developed and tested for its use in microwave head imaging; however, these antennas are unsuitable for wearable systems due to their high-profile structure. A low-profile and compact antenna was investigated in [9], but has the disadvantage of using rigid materials that does not allow it to be conformal to the head. In [10] and [11], flexible antennas have been proposed for wearable head imaging applications utilising thin FR-4 and polyethylene terephthalate (PET) substrate. A fully textile wideband antenna is proposed in [12] for microwave medical imaging. However, the size of the antenna is large and is not suitable to be used as an array element. In [13], a study was performed on the design of a polydimethylsiloxane (PDMS) embedded conductive fabric patch antenna for wearable applications. The design and performance of the antenna is promising; however, it was only applied on the arm and therefore would not be optimal for head imaging due to the different layers of tissues in the head. Finally, in [14], a flexible wideband antenna array was developed for stroke detection that uses several layers of PDMS that embeds a copper radiating layer etched on a polyimide film substrate. The flexible nature of the antenna allowed it to conform to the head and it was able to detect the presence of stroke.

Since a typical VNA contains only two ports, each port can only be connected to one antenna at a time. Therefore, depending on the number of antennas in a microwave medical system, obtaining data from each antenna can be a time-consuming process as each antenna needs to be connected to the VNA one at a time. In order to speed up the data acquisition time, a switching system is a convenient feature to have that allows the device to switch between each antenna elements that are connected to the VNA ports quickly. In [15], a microwave head imaging system was reported that consisted of 16 Vivaldi antennas positioned around a head phantom and using a switching system. The switching system developed in this work utilized coaxial switches in order to connect the elements of the array. However, the size of the switching system is relatively large and only suitable for static testing environments. A low cost and compact RF switching system was developed and presented in [16]. This system used two monolithic microwave integrated circuits (MMIC), each consisting of a one-pole four-throw (1P4T) switch in combination with a one-pole eight throw (1P8T) switch that allowed the microwave head device to obtain reflection coefficient (S_{11}) and transmission coefficient (S_{21}) separately. In addition, the system was controlled by a Bluetooth module that allowed the user to automatically choose which antennas were active using a mobile app developed on Android. Although the system is low cost, compact, and light, its circuit was implemented on a PCB which makes it difficult to conform to curves surfaces. As a result, the switching circuit would need to be placed somewhere on top of the device and easily accessible to all the antennas, thus limiting its space.

In this paper, hybrid silicone-textile sensors were developed that propagates at dual resonant frequencies: 800 MHz and 2.1 GHz respectively. The sensors were developed based on a rectangular planar monopole antenna structure. In addition, a flexible, low-cost switching system is developed and used with the sensors. The switching system was developed on a flexible protoboard and consists of one-pole one throw (1P1T) switches and a SMA breakout board. The sensors and switching system were then integrated into a wearable hat-like device and used to monitor brain atrophy and lateral ventricle enlargement, which are two common physiological changes associated with neurodegenerative diseases. The sensor's ability to resonate at dual frequencies provides a means of detecting brain atrophy and lateral ventricle enlargement separately. The flexible switching system also successfully changed between each of the active sensors. Artificial head phantoms were fabricated to represent brain atrophy and lateral ventricle enlargement. Reflection coefficients (S_{11}) of the flexible antenna sensors were captured and analyzed to determine whether the fabricated sensor could detect different levels of neurodegeneration based on the amount of brain atrophy and lateral ventricle enlargement in the brain.

II. Design and Fabrication Methodology

A. Flexible Dual Resonant Sensor Design and Fabrication

The design of the sensor is shown in Fig. 1 and is based off a rectangular planar monopole antenna structure. The conducting material of the sensor is fabricated using a 0.1-mm-thick flexible conductive textile, Shieldex Zell that has a surface resistance (R_{sq}) that is less than 0.02 Ω. The substrate of the sensor was made using Shore A8 silicone rubber due to its ability to flex and stretch without breaking its overall structure. The silicone rubber has a measured relative permittivity, ε_r and loss tangent, $tan\,\delta$ of 2.99 and 0.032 respectively. In addition, it has a tensile strength of 218 psi and a tear resistance of upto 20 ppi.

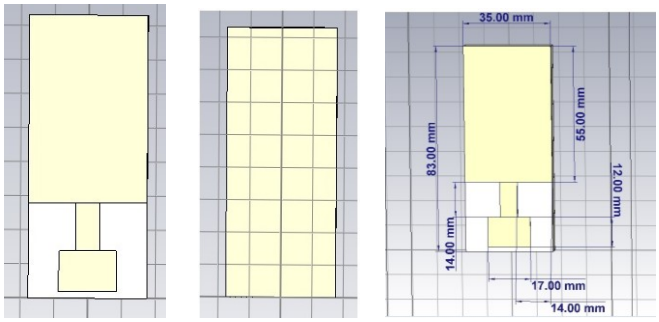

Fig. 1 a) Top view and b) Bottom view of the proposed hybrid silicone-textile sensor along with (c) its geometrical dimensions.

Computer model simulations of the sensor were carried out using CST Microwave Suite. Simulations were performed using difference length and width sizes for the sensor in order to obtain the optimal size that allows the sensor to propagate at the required dual resonant frequencies. In addition, the thickness of the substrate was also optimised in order to design a sensor that gives very little backward-propagated radiation. The final dimensions of the designed sensor are shown in Fig. 1(c) that allows it to resonate at 800 MHz and 2.1 GHz respectively. The fabrication method of the sensor is shown in Fig. 3. First, a 1 mm silicone rubber mold was created. After the mold cured, the ground plane of the sensor was placed on top. 3 mm of silicone rubber was then poured on the sensor and cured. Once cured, the rectangular monopole patch of the sensor was then placed on top the structure and another 1 mm of silicone rubber was poured on the structure. After the overall structure was cured, a slot was made at the feeding line and ground plane side. A SMA connector was then attached to the sensor using silver epoxy.

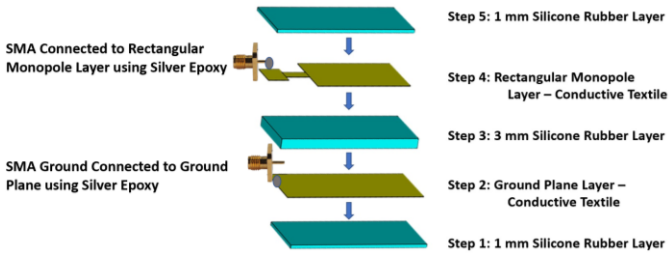

Fig. 3 Diagram showing the different layers of the fabricated hybrid silicone-textile sensor.

The sensor is fed with a microstrip line where the line is then transitioned into a rectangular monopole structure. In order to improve the directionality of the sensor, the ground plane is placed at a distance of 3 mm away from the patch so that it reflects the backward propagated RF signals in the forward direction. The prototype of the proposed textile antenna is shown in Fig. 4.

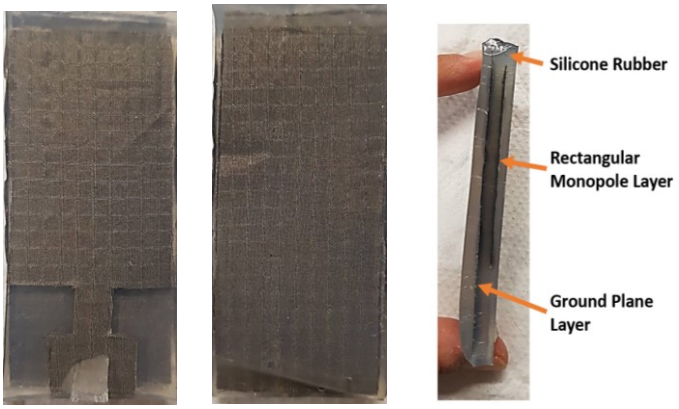

Fig. 4. Top, bottom, and side view of the fabricated hybrid silicone-textile sensor.

B. Flexible Switching Circuit Design and Fabrication

In order to conveniently and easily switch between each sensor, a flexible switching circuit was developed. The switching circuit consists of four SMA connectors and three 1P1T switches. Three SMA connectors are connected to the antennas on one side of the wearable device. The fourth SMA connector is connected to a port of the VNA. The 1P1T switches controls which sensor is active. This is manually controlled and only one switch should be turned on at a time in order to avoid shorting the circuit. Fig. 5 shows a block diagram of the overall microwave wearable device and the integration of the sensors (called Ant 1, Ant 2, …, Ant 6) and flexible switching circuit.

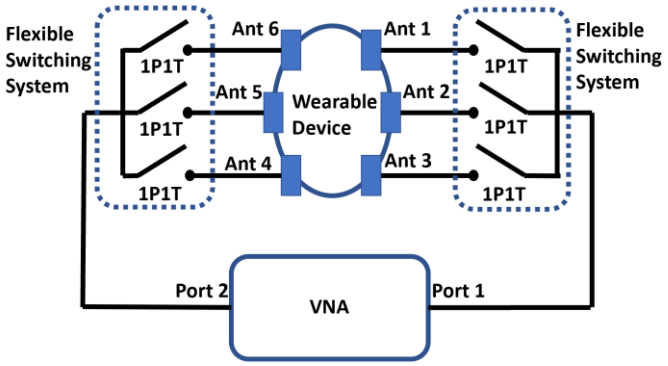

Fig. 5. Block diagram of the overall microwave wearable device which has the flexible sensors (labelled as Ant 1, Ant 2, …, Ant 6) and flexible switching circuit integrated.

The flexible switching circuit was developed on a flexible perma-protoboard from Adafruit. The protoboard is made from a thin polyamide film and has dimensions of 78.88 mm x 43.26 mm. The protoboard weighs 0.65 g and has a bend radius of 1 cm. By using this protoboard, the switching circuit has the ability to conform to the contours of the wearable device used in the experiments. 4 SMA breakout boards from Atlas Scientific were placed on each perma-protoboard so that it can connect 3 sensors with the VNA. All the connections switches and SMA connectors of the perma-protoboard were soldered in place. Figs. 6(a)-(c) shows the front, back, and side view of the developed switching circuit respectively, while Fig. 6(d) shows switching circuit being bent.

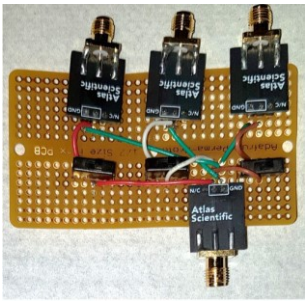

(a)

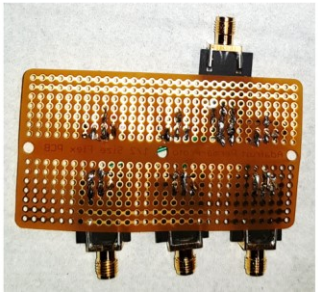

(b)

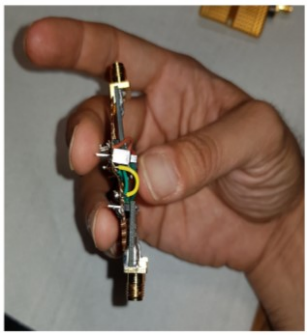

(c)

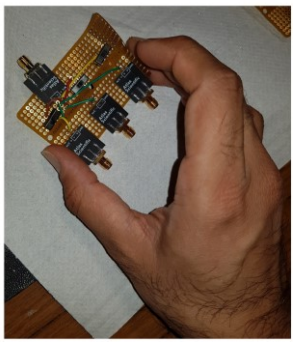

(d)

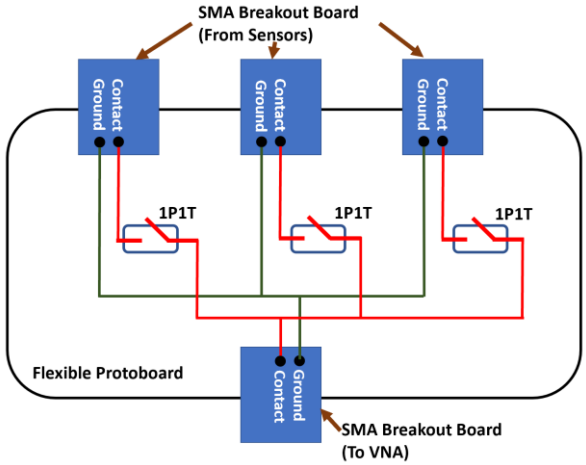

(e)

Fig. 6. (a) Top view, (b) rear view, (c) side view of the assembled flexible switching circuit, (d) switching circuit being bent, and (e) schematic diagram of the flexible switching circuit.

III. Experimental Setup

The sensors and switching circuit were integrated into a wearable hat-like structure shown in Figs. 7(a)-(b). Six sensors were placed inside the inner lining of the cap and the two flexible switching circuits were placed on the external sides of the hat structure such that they could be easily accessible to the sensors. SMA cables were then used to connect each sensor with the SMA connectors on the switching circuit. The weight of the different components in the wearable device are given in Table I.

(a)

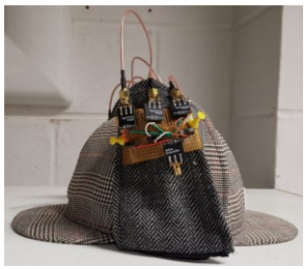

(b)

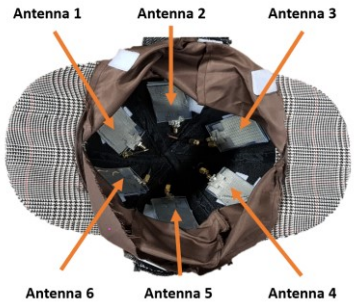

(c)

Fig. 7. (a) Front view, (b) side view, and (c) inner view of the wearable neurodegeneration monitoring device with flexible sensors and switching circuit integrated on it.

TABLE I
Approximate Weights of Different Components in Wearable Device

Components	Weight (g)
Deerstalker Hat	259
Switching Circuit (Protoboard + Switches + SMA Breakout Board)	3
Sensor	4.45
Total (Hat + 2x Switching Circuit + 6x Sensors)	291.7

The experimental setup is shown in Fig. 8 and comprises of a VNA, a wearable device containing 6 hybrid silicone-textile sensors and 2 flexible switching circuits, host PC, and the skull model which contains biophantoms that mimic properties of the brain during neurodegenerative diseases (i.e. with different levels of brain atrophy and lateral ventricle enlargement).

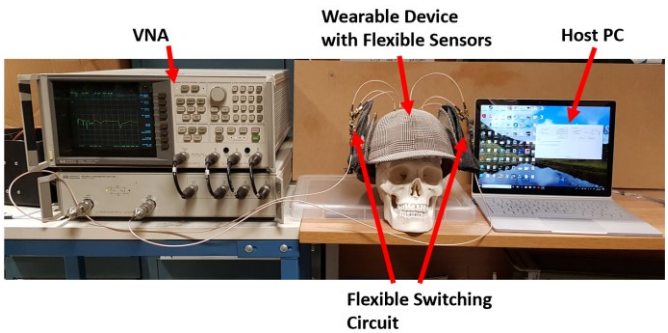

Fig. 8. Screenshot of the experimental setup used to test proposed sensor.

The host PC was connected to the VNA via a GPIB that allows users to send commands to the VNA to start generating signals and capture S_{11} data from the port directly into the PC using a built-in software. The VNA used in the experiments is a HP 8753 that has a frequency range of 300 kHz to 3 GHz with a dynamic range of up to 100 dB. One SMA connector on each of the switching circuits were connected to one of the 50-ohm ports on the VNA using SMA cables. S_{11}, or reflection coefficient, data was then captured at the same port and processed on the PC for each antenna by turning on the switch associated with the active element and keeping the other switches off. Biophantoms mimicking the dielectric properties of the brain were fabricated based on a method given in [17]. 700 mL of tap water was mixed with 600 mL of sugar, and 100 mL of agar powder. The total volume for the biophantom would equal 1400 mL, which corresponds to the total brain volume of an average adult human [11].

In order to detect the progress of neurodegeneration in the brain, two important changes need to be detected: 1) brain atrophy, or shrinking of the brain volume, and 2) lateral ventricle enlargement. In order to mimic the characteristics of brain atrophy, several biophantoms of different sizes and volumes were created and placed into the skull model. In addition to brain atrophy, the characteristic of lateral ventricle enlargement was also mimicked in the experiments by creating samples of different sizes using solidified coconut oil to represent cerebrospinal fluid (CSF) that accumulate in the lateral ventricles as they enlarge. CSF has a measured relative permittivity in the range of 70 to 68.9 between 500 MHz and 800 MHz [20]. The solidified coconut oil, on the other hand, has a maximum relative permittivity of 36.4. In order to match the dielectric properties between the solidified coconut oil samples and CSF, the coconut oil was mixed with salt. In particular, for mild neurodegeneration, around 36 ml of salt was mixed with 56 ml of coconut oil to create the CSF phantom used in the experiment. Similarly, in the case of severe neurodegeneration, around 96 ml of salt was mixed with 150 ml of coconut oil to create the CSF phantom used in the experiment. This method was used based on the work performed in [7] where the authors fabricated different sizes of CSF objects to simulate the characteristic of enlarged lateral ventricles. Although the fabricated CSF objects do not accurately represent the fluidic nature of CSF, the samples provide a convenient way of performing the experiments for lateral ventricle enlargement to evaluate the performance of the sensors and switching circuit. It should be noted that the actual geometry of lateral ventricles in the brain is much more complex than the sphere object that is used in the experiment; therefore, the CSF distribution will also match this complex geometry in real-life and thus the measured S-parameters will also be different. In particular, due to the S-parameters being affected by changes in dielectric constants, there could be variations in S_{11} measurements at other frequencies that correspond to some of the ventricles in the brain that are relatively closer to the sensor than the cases used in the experiments. Nonetheless, it is important to note that CSF has a higher dielectric constant compared to gray and white matter. Therefore, regardless of the geometry of the CSF distribution, the S-parameters will still change significantly when there is an increase in CSF volume in the brain, especially in the lateral ventricles.

For this study, experiments were performed on three cases: 1) Normal brain (i.e. no neurodegeneration, 2) Mild neurodegeneration that is characterized by 10% brain atrophy and 56 mm^3 increase of CSF in the lateral ventricles, and 3) Severe neurodegeneration that is characterized by 25% brain atrophy and 150 mm^3 increase of CSF in the lateral ventricles. These levels of brain atrophy and lateral ventricle enlargement were chosen based on whole-brain atrophy and lateral ventricle enlargement rates obtained in [1]-[4]. Since the study mainly focused on evaluating the sensors and switching circuit, rather than fabricating several phantoms to simulate neurodegeneration for each year, it was decided to develop phantoms that mimicked key stages of neurodegeneration (i.e. mild and severe). The case of mild neurodegeneration can be associated to a patient who has been suffering from neurodegeneration for 4 to 5 years, while severe neurodegeneration can be associated with a patient suffering from the disease for 9 to 10 years. Table II shows the volumes of the brain and CSF phantoms that were used for each of the cases. Figs. 9 (a) and (b) shows screenshots of biophantom representing the brain and CSF respectively.

TABLE II
VOLUMES OF BRAIN AND CSF PHANTOMS USED IN EXPERIMENTS

Cases	Brain Volume (mL)	CSF Volume (mm^3)
Normal (Control)	1400	0
Mild Neurodegeneration	1260	56
Severe Neurodegeneration	1050	150

(a) (b)

Fig. 9. Screenshot of the fabricated phantom that was used to mimic characteristics of a) human brain and b) CSF that accumulates in lateral ventricles.

IV. RESULTS

A. Simulation Results

The performance of the sensor was validated and optimised using CST Microwave Studio. Based on the simulations, the designed sensor's operating frequencies were found to be at 1.1

GHz and 2.65 GHz. Far-field simulations were conducted to calculate the sensor's front-to-back (FTB) ratio to ensure that the sensor could block any signals coming outside the object of interest and mainly focus on receiving signals from the brain. The simulated FTB ratio of the proposed sensor at both the resonant frequencies is approximately 4 dB at 1.1 GHz and 6 dB at 2.65 GHz, thus confirming its directional characteristic.

In addition, numerical simulations were conducted to investigate the transmitted electromagnetic wave across the operating bandwidth of the proposed antenna inside the head. Between 800 MHz and 1.1 GHz, the electromagnetic waves were found to propagate to the region associated with the lateral ventricles. Between 1.8 GHz and 2.65, the propagated electromagnetic waves were found to be mostly absorbed in the gray matter regions of the brain. After fabrication of the sensor, S_{11} data was measured and compared with the S_{11} data obtained in the simulations and shown in Fig. 10.

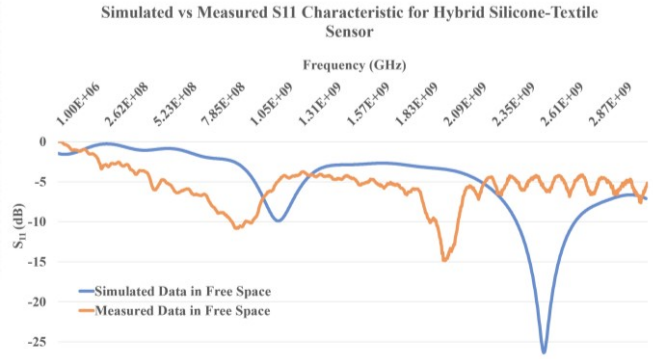

Fig. 10. Simulated vs. measured reflection coefficients of the sensor in free space.

It can be seen that the measured S_{11} data for the fabricated sensor is slightly different from the simulated S_{11} measurements, where the first resonant frequency is at 800 MHz and the second resonant frequency is between 1.8 and 2.09 GHz. This difference can be due to differences in the fabricated geometry of the sensor, noise in the environemnt, or due to highly flexible nature of the fabricated sensor when obtaining the measurements with the VNA. In any case, the S_{11} measurement for the fabricated sensor is still acceptable for this experiment.

B. Experimental Results - Sensors

Experiments were performed using the setup and fabricated phantoms as described in Section III. In order to validate that the sensor's ability to detect brain atrophy and lateral ventricle enlargement separately, two experiments were performed. First, a smaller brain phantom was placed in the skull model and its corresponding S_{11} was measured. Then a large CSF sample was placed in the normal brain phantom and its corresponding S_{11} was captured. The resulting plot is shown in Fig. 11.

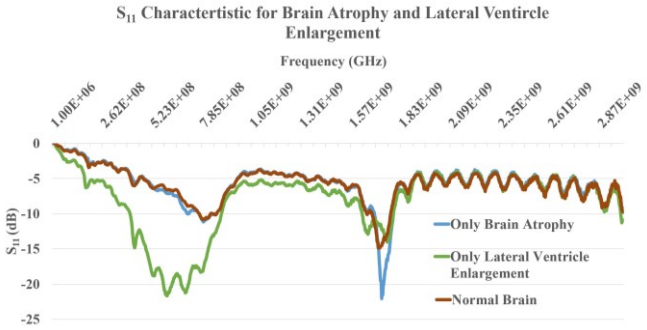

Fig. 11. Reflection coefficient (S_{11}) measurements obtained from experiments that measure brain atrophy and lateral ventricle enlargement separately.

It can be seen that when brain atrophy is present, there is a higher loss in the reflection coefficient (S_{11}) at around 1.78 GHz, which is close to the sensor's higher resonating frequency range between 1.8 and 2.09 GHz. In addition, when the CSF sample is placed in the normal brain, emulating the enlargement of lateral ventricle, then the reflection coefficient has a higher loss between 400 to 800 MHz. Thus, this proves the validity of the dual resonant nature of the sensor and its ability to differentiate between detecting brain atrophy and lateral ventricle enlargement successfully. In addition, it can be seen that outside of these ranges, the characteristic of the reflection coefficient for both brain atrophy and lateral ventricle enlargement matches with the characteristic of a normal brain phantom.

The second experiment focused on validating the sensor's ability to differentiate between different levels of neurodegeneration using the phantoms discussed in Section III. In the experiment, S_{11} data was measured at: 1) free space, 2) with normal brain phantom, 3) mild neurodegeneration, and 4) severe neurodegeneration. Mild and severe neurodegeneration were simulated using brain phantoms and CSF samples that were fabricated with the volumes shown in Table 1. To simulate lateral ventricle enlargement, the CSF samples were inserted into the brain phantoms and placed in the skull model. Fig. 12 shows the resulting reflection coefficient plots that were obtained in this experiment.

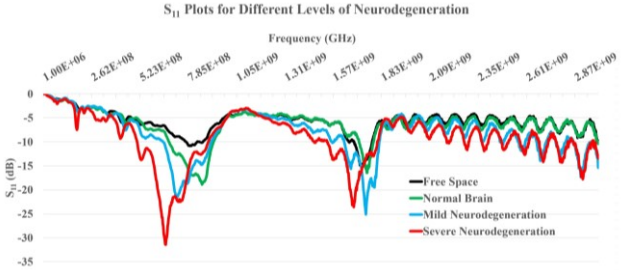

Fig. 12. Measurements of reflection coefficient (S_{11}) that were obtained from experiments for 1) free space, 2) normal brain, 3) mild neurodegeneration, and 4) severe neurodegeneration.

It can be seen in Fig. 12 that as the level of neurodegeneration increases in the brain, there is a significant loss in the reflection coefficient that occurs between 500 to 800 MHz and 1.57 to 1.8 GHz. In addition, the amount of loss for the reflection coefficient at both frequency ranges increase as brain atrophy and volume of CSF in the lateral ventricle region increases. The result from this plot confirms that the proposed sensor is

capable of detecting the level of neurodegeneration in the brain. In addition, dual resonant frequency ranges of the sensor ensure that brain atrophy and lateral ventricle enlargement can be monitored separately.

The resulting plots in Figs. 11 & 12 were generated by switching one sensor "on", while keeping the other sensors "off," and capturing the S_{11} data from it. This would be repeated for all the six sensors. Once S_{11} data was captured from the six sensors, the results were averaged and the mean S_{11} value for each frequency was plotted. In addition, the variance for both Fig. 11 and Fig. 12 was calculated to be 37.89 and 50.064 respectively.

C. Experimental Results – Switching Circuit

In the final set of experiments, the flexible switching circuit was tested to verify the performance of the 6 1P1T switches that are used for each sensor. In particular, measurements were taken using the VNA in order to capture the insertion loss and return loss for each switch. Insertion loss is the total power lost through the insertion of a device (in this case, a switch) in a transmission line. The insertion loss for switches is captured in its "on" state and is considered a critical parameter in designing switching circuits, as it provides an indication of how much noise is added into the system. Return loss is the loss of power in the signal reflected by a device (i.e. a switch) in a transmission line. This parameter is also important in designing switching circuits as it gives an indication of how well devices or lines are matched. In order to calculate the insertion and return loss for the switching circuits, first the S-parameters were measured for the 1P1T switches using the VNA. Then, S_{11} and S_{21} were used in the following equations to calculate insertion and return loss respectively:

$$Insertion\ Loss\ (dB) = -20\ log_{10}|S_{21}| \quad (1)$$

$$Return\ Loss\ (dB) = -20\ log_{10}|S_{11}| \quad (2)$$

where S_{11} and S_{21} are the reflection and transmission coefficients, respectively. The plots of the insertion and return losses for the 6 1P1T switches are shown in Figs. 13 and 14.

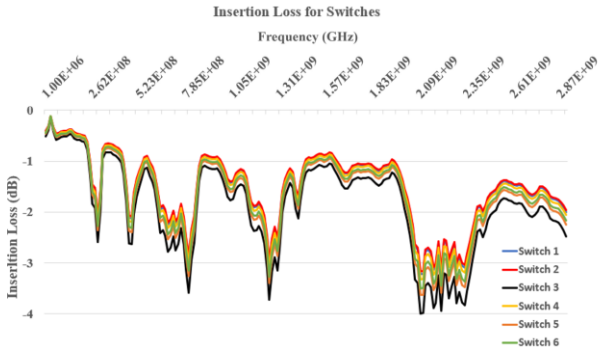

Fig. 13. Measured insertion loss in dB for the 6 1P1T switches.

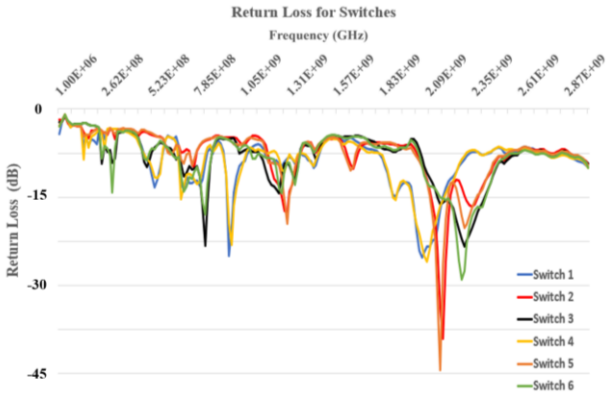

Fig. 14. Measured return loss in dB for the 6 1P1T switches

The plot in Fig. 13 indicates that for all the switches, the insertion loss does not exceed more than -3.9 dB for all the switches across the frequency range. In addition, it can be seen that in the frequency ranges of around 0.8 MHz to 1.2 GHz and 1.57 GHz to 1.85 GHz, the insertion loss is not less than -2 dB. This provides the indication that the designed switching circuit is good and that not too much unwanted noise or reflections will be generated by the switches in the region of the dual resonant frequencies of the sensors. In addition, the plots for return loss in Fig. 14 shows that all the switches match relatively well due to the high return loss values across the frequency spectrum. Future work will be undertaken to enhance the design and fabrication of the switching circuit to ensure that connections are secured and do not vibrate or cause noise when being worn by the user.

The proposed wearable device with integrated flexible sensors and flexible switching circuit is compact, light-weight, portable, and uniquely design to have all components integrated onto a hat-like structure, compared to other microwave head imaging systems in [14], [15], and [16]. Compared to the other microwave head imaging systems, the switching circuit developed in this paper has a slightly higher maximum insertion loss as compared to other papers. This can be due to the flexible nature of the board and soldering effects that may cause traces to touch one another, as compared to the more rigid switching circuits that were developed in [15] and [16] respectively. However, the insertion loss is still low enough to satisfy our requirements and validate the switches performance in not introducing too much noise into the system. The flexible sensors that were fabricated in this paper are unique compared to those in [14], [15], and [16], in that it has the capability of detecting two separate physiological changes in the brain due to its dual resonating frequencies. This differentiates from the other flexible sensors designed in [14] and [16], where they had UWB characteristics to detect the presence of stroke at a certain location in the brain. The data acquisition time is approximately 3 minutes, which is significantly faster than MRI and CT scans that normally take 10 to 30 minutes to complete [18]. The wearable device also has the advantage of being non-ionising, low-power, and low cost, making it safe, easy, and convenient for patients suffering from neurodegenerative diseases to use for quick monitoring and diagnosis. However, the imaging capability has not been developed yet and future work needs to be done in order to provide high resolution images along the lines of what is generated from MRI and CT scans. Table III

shows a benchmark comparison of this device with conventional medical devices used for detecting brain atrophy and lateral ventricle enlargement [19].

TABLE III
COMPARISON OF IMAGING TECHNIQUES FOR BRAIN ATROPHY AND VENTRICLE ENLARGEMENT

Imaging System	Advantages	Disadvantages
MRI	- High Image Resolution - Non-ionizing	- Expensive - Bulky - Uncomfortable and Difficult for Patients - Slow Scan Times
CT Scan	- High Image Resolution	- Expensive - Bulky - Uncomfortable - Ionizing
Wearable Device (in this work)	- Low Cost - Fast Scan Times - Nonionizing - Wearable - Portable - Comfortable - Safe	- No images

V. CONCLUSION

A flexible and wearable hybrid silicone-textile sensor and switching system was presented. The sensor consists of a rectangular monopole feeding line and a ground plane that was made of conductive textile and embedded in a silicone-rubber mold substrate. The sensor obtained a dual resonant frequency, one between 600 and 800 MHz, and the other between 1.8 to 2.09 GHz. The sensors and switching circuit could be integrated into a wearable device successfully. The flexible nature of the materials used to develop these two components allowed them to be conformal to the round hat-like structure and therefore be wearable. Experimental results show that the designed sensor was able to capture and differentiate between brain atrophy and lateral ventricle enlargement successfully, both pathological effects that are commonly associated with neurodegenerative diseases. In addition, the loss in measured S_{11} data for the sensor differs for increasing levels of neurodegeneration. The switching circuit also successfully switched between each sensor that was used by the VNA and obtained the right readings. This provides a unique, compact, low cost, and flexible sensor that has the potential of being used for medical diagnostic systems. Future work will be performed in order to enhance the experiments by creating more realistic phantoms to emulate the physical properties of brain tissues, ventricles, and CSF respectively. In addition, the authors plan to evaluate the wearable device for monitoring different neurodegenerative diseases, such as Alzheimer's disease and Lewy Body Dementia.

REFERENCES

[1] J. D. Sluimer, H. Vrenken, M. A. Blankenstein, *et al*, "Whole-brain atrophy rate in Alzheimer disease: identifying fast progressors," *Neurology*, vol. 6, no. 70, 2008, pp. 1836-1841.

[2] G. Spulber, E. Niskanen, S. MacDonald, *et al*, "Whole brain atrophy rate predicts progression from MCI to Alzheimer's disease," *Neurobiology of Aging*, vol. 31, no. 9, 2010, pp. 1601-1605.

[3] S. Nestor, R. Rupsingh, M. Borrie, M. Smith, V. Accomazzi, J. Wells, J. Fogarty, R. Bartha, and ADNI, "Ventricular enlargement as a possible measure of Alzheimer's disease progression validated using the Alzheimer's disease neuroimaging initiative database," *Brain*, **131**, (9), 2008, pp. 2443-2454.

[4] O. T. Carmichael, L. H. Kuller, O. L. Lopez, *et. al.*, "Cerebral Ventricular Changes Associated with Transitions Between Normal Cognitive Function, Mild Cognitive Impairment, and Dementia," *Alzheimer Dis. Assoc. Disord.*, **21**, (1), 2007, pp. 14-24.

[5] Mohammed, B.J., Abbosh, A.M., Mustafa, S., Ireland, D.: 'Microwave system for head imaging'*IEEE Trans. Instrum. Meas.*, 2014, **63**, (1), pp. 117–123.

[6] Mobashsher, A.T., Member, S., Abbosh, A.M., Member, S., Wang, Y.: 'Microwave system to detect traumatic brain injuries using compact unidirectional antenna and wideband transceiver with verification on realistic head phantom'*IEEE Trans. Microw. Theory Tech.*, 2014, **62**, (9), pp. 1826–1836.

[7] I. Saied and T. Arslan, "Non-invasive Wearable RF Device towards Monitoring Brain Atrophy and Lateral Ventricle Enlargement," *IEEE Jour. Of Electromagnetics, RF, & Microw. For Med. & Biol.*, 2019. doi: 10.1109/JERM.2019.2926163

[8] Mobashsher, A.T., Abbosh, A.M.: 'On-site Rapid Diagnosis of Intracranial Hematoma using Portable Multi-slice Microwave Imaging System'*Sci. Rep.*, 2016, **6**, (1), p. 37620.

[9] Jalilvand, M., Zwick, T., Wiesbeck, W., Pancera, E.: 'UWB synthetic aperture-based radar system for hemorrhagic head-stroke detection'*2011 IEEE RadarCon*, 2011, pp. 956–959.

[10] Bashri, M.S.R., Arslan, T., Zhou, W., Haridas, N.: 'Wearable device for microwave head imaging', in '46th European Microwave Conference (EuMC)' (2016), pp. 671–674

[11] Bashri, M.S.R., Arslan, T., Zhou, W.: 'Flexible Antenna Array for Wearable Head Imaging System', in '11th European Conference on Antennas and Propagation (EUCAP)' (2017), pp. 172–176.

[12] Soh, P.J., Van Den Bergh, B., Xu, H., *et al.*: 'A smart wearable textile array system for biomedical telemetry applications'*IEEE Trans. Microw. Theory Tech.*, 2013, **61**, (5), pp. 2253–2261.

[13] R. Simorangkir, Y. Yang, R. Hashmi, T. Bjorninen, K. Esselle, and L. Ukkonen, "Polydimethylsiloxane-Embedded Conductive Fabric: Characterization and Application of Robust Passive and Active Flexible Wearable Antenna," *IEEE Access*, vol. 6, pp. 48102-48112, 2018.

[14] A. S. M. Alqadami, K. Bialkowski, A. T. Mobashsher, and A. Abbosh, "Wearable Electromagnetic Head Imaging System Using Flexible Wideband Antenna Array Based on Polymer Technology for Brain Stroke Diagnosis," *IEEE Trans. Biomed. Circuits and Systems*, vol. 13, no. 1, pp. 124-134, 2019.

[15] B. J. Mohammed, A. M. Abbosh, S. Mustafa and D. Ireland, "Microwave System for Head Imaging," in *IEEE Transactions on Instrumentation and Measurement*, vol. 63, no. 1, pp. 117-123, Jan. 2014.

[16] M. S. R. Bashri and T. Arslan, "Low-cost and compact RF switching system for wearable microwave head imaging with performance verification on artificial head phantom," in *IET Microwaves, Antennas & Propagation*, vol. 12, no. 5, pp. 706-711, 18 4 2018.

[17] Candefjord, S., Winges, J., Malik, A.A., *et al.*: 'Microwave technology for detecting traumatic intracranial bleedings: tests on phantom of subdural hematoma and numerical simulations'*Med. Biol. Eng. Comput.*, 2016, pp. 1–12.

[18] C. S. Kidwell, J. A. Chalela, et al., "Comparison of MRI and CT for detection of acute intracerebral hemorrhage," *Jama Network*, vol. 2, no. 929, pp. 1823-1830

[19] J. T. Bushberg, J. A. Seibert, E. M. Leidholdt, J. M. Boone, *The Essential Physics of Medical Imaging*, Lippincott Williams & Wilkins, Philadelphia, USA, 2011.

[20] C. Gabriel, S. Gabriel, and E. Corthout, "The dielectric properties of biological tissues: II. Measurements in the frequency range 10 Hz to 20 GHz," Phys. Med. Biol., Vol. 41, pp. 2231-2249, 1996.

Imran M. Saied obtained his B.Sc. in Electrical Engineering from Georgia Institute of Technology in 2009 and his M.Sc. in Electrical Engineering from California State University-Fullerton in 2011. He is currently pursuing his PhD at the University of Edinburgh, where he focuses his research on investigating the use of RF and microwaves for detecting neurodegenerative diseases.

He has an extensive global work experience spanning across U.S.A., India, and U.A.E. Prior to beginning his PhD, he worked as a Research Assistant for the Petroleum Institute (now Khalifa University) in Abu Dhabi, U. A. E. from 2013 to 2017. He worked on developing several tomography and spectroscopy systems for real-time oil and gas pipeline monitoring systems. In particular, he focused on THz spectroscopy, ECT/ECAT tomography, and development of sensors and imaging algorithms for these systems. The results that have been obtained from his work have led to several refereed journal and conference papers that have been published in IEEE and SPE.

Prof. Siddharthan Chandran holds the MacDonald Chair of Neurology in the Centre for Clinical Brain Sciences, University of Edinburgh, Edinburgh, UK. He works in the emerging discipline of Regenerative Neurology. His research combines laboratory activity that includes human stem cells with specialist clinics to both study several neurodegenerative diseases as well as undertake early-phase clinical trials.

Prof. Chandran is also the Director of the Anne Rowling Regenerative Neurology Clinic and Programme Lead of the UK Dementia Research Institute at the University of Edinburgh where he leads and develops research activities and clinical experimental infrastructure for longitudinal studies.

Prof. Tughrul Arslan holds the Chair of Integrated Electronic Systems in the School of Engineering, University of Edinburgh, Edinburgh, UK. He is a member of the Integrated Micro and Nano Systems (IMNS) Institute and leads the Embedded Mobile and Wireless Sensor Systems (Ewireless) Group in the University (ewireless.eng.ed.ac.uk). His current research focuses on developing low power radio frequency sensors for wearable and portable biomedical applications. He is the author of over 500 refereed papers and inventor of over 20 patents.

Prof. Arslan is currently an Associate Editor of IEEE Transactions on VLSI Systems and was previously an Associate Editor for the IEEE Transactions on Circuits and Systems I (2005-2006), IEEE Transactions on Circuits and Systems II (2008-2009). He is also a member of the IEEE CAS executive committee on VLSI Systems and Applications (1999 to date), and is a member of the steering and technical committees of a number of international conferences. He is a co-founder of the NASA/ESA conference on Adaptive Hardware and Systems (AHS) and currently serves as a member of its steering committee.